

# A Magnetorheological Damper with Embedded Piezoelectric Force Sensor: Experiment and Modeling

Y. Q. Ni and Z. H. Chen

*Department of Civil and Structural Engineering, The Hong Kong Polytechnic University  
Hong Kong, China*

## 1. Introduction

Semiactive control systems that offer the reliability of passive control systems as well as the versatility and adaptability of active control systems have received significant attention for structural vibration control (Jung et al., 2004). Magnetorheological (MR) fluid dampers have emerged as such a class of semiactive damping devices. By activating the MR fluid contained in the device through magnetic field, it can reversibly change from liquid to semisolid in milliseconds, which results in a continuously controllable device with high bandwidth. Moreover, MR dampers require minute power for the field activation and are insensitive to impurity penetration such as are commonly encountered during manufacture and usage (Carlson et al., 1996). More importantly, they are inherently fail-safe devices in that they can still operate as passive dampers once the control hardware fails. Recognizing the attractive characteristics and promising potential of the MR-based damping technique, numerous researchers and engineers have investigated the feasibility and application of the MR dampers in a wide variety of areas, such as seismic protection of building and bridge structures (Dyke et al., 1996; Gordaninejad et al., 2002; Loh et al., 2007), vibration control of bridge cables (Johnson et al., 2000; Ko et al., 2002; Ni et al., 2002; Duan et al., 2005; Weber et al., 2005b; Li et al., 2007), vibration damping of suspension systems of trains and vehicles (Liao and Wang, 2003; Song et al., 2005; Choi et al., 2009), and stability augmentation of helicopters (Gandhi et al., 2001; Hu & Wereley, 2008).

While possessing controllable damping capability, the existing MR dampers are incapable of monitoring structural vibrations or excitations exerted on structures, and require extra sensors for implementing closed-loop semiactive control. As a consequence, the MR dampers are usually used as adjustable passive dampers in an open-loop mode in the current practices of civil structural control, like in vibration control of bridge cables (Chen et al., 2004; Weber et al., 2005a), which hinders full utilization of their controllable damping capability. Recently, a self-sensing MR damper embedded with a piezoelectric force sensor has been developed to possess dual functionality of force sensing and controllable damping; thus it has the potential to facilitate real-time closed-loop control in a relatively simple and cost-effective manner (Or et al., 2008).

One of the important tasks to fully exploit the potential of an MR damper in control implementation is to establish an accurate model that can characterize its intrinsic highly

Source: Vibration Control, Book edited by: Dr. Mickaël Lallart,  
ISBN 978-953-307-117-6, pp. 380, September 2010, Sciyo, Croatia, downloaded from SCIYO.COM

nonlinear properties, particularly hysteresis and force saturation. On the other hand, in well recognizing the fact that the force generated by the MR damper cannot be controlled directly and only the current applied to the MR damper can be commanded, it is essential and beneficial to build a model for describing the inverse dynamics of the MR damper. The inverse dynamic model will be incorporated into the control system to produce currents for the MR damper to track the desired optimal control forces implementable by the damper.

Since the last decade, considerable research efforts have been devoted to representing the forward dynamics of MR dampers and a variety of models have been documented in the literature. They can be classified as parametric and nonparametric models. Among several parametric models described in terms of analogous mechanical elements (Kamath & Wereley, 1997; Wereley et al., 1998; Spencer et al., 1997; Jiménez & Álvarez-Icaza, 2005; Ikhouane & Dyke, 2007), a phenomenological model on the basis of the Bouc-Wen hysteresis model proposed by Spencer et al. (1997) is regarded as the “state-of-the-art” semi-physical model of an MR damper. This model can accurately represent the nonlinear hysteresis of a typical MR damper over a wide range of operating conditions. However, it includes fourteen parameters in need to be adapted; identification of them requires sophisticated searching algorithms and is computationally intense. Also, a high integration-step rate in the order of kHz has to be used to ensure numerical stability in solving the nonlinear differential equations, which limits the model’s application in real-time control.

An alternative representation of forward dynamics of MR dampers is by using nonparametric methods, especially black-box modeling techniques, due to their considerable flexibility and effectiveness in system modeling as well as few physical insights necessary for developing a model. These black-box techniques include adaptive neuro-fuzzy inference system (Schurter & Rochke, 2000), polynomial NARX (nonlinear autoregressive with exogenous inputs) modeling (Leva & Piroddi, 2002), wavelets-based identification technique and ridgelet network optimization approach (Jin et al., 2005), and artificial neural networks (Chang & Roschke, 1998; Wang & Liao, 2001; Du et al., 2006; Cao et al., 2008). Despite the widespread use of the black-box techniques in MR damper modeling, only a few models were developed and evaluated based on real measurement data of MR dampers and using numerical simulation data instead. Moreover, it is commonly believed that neural networks are prone to overfitting, which occurs when a neural network only memorizes the superficial details of training data rather than learns the true relationship underlying the data. Hence, generalization capability is a critical concern in constructing a neural network for estimation or prediction on novel situations. However, few of the previous works addressed the overfitting or generalization issue when using neural networks to identify the dynamics of MR dampers, which might give rise to reliability problem in the control applications with the overfitted black-box models.

Likewise, due to the highly nonlinear properties of an MR damper, a linear forward parametric model invertible for determining command current to be input into the MR damper is not available; and what is more, it is challenging to formulate a nonlinear parametric model for the inverse dynamics similar to a forward one. Tsang et al. (2006) developed simplified inverse dynamics (SID) models for MR dampers with respect to the Bingham plasticity model and the Bouc-Wen hysteresis model (Spencer et al., 1997) using a piston velocity feedback algorithm and a damper force feedback algorithm for each model. The effectiveness of the SID models was demonstrated in terms of force tracking accuracy through numerical simulations, while errors exist in the pre-yielding phase when the damper piston velocity is small. More recently, attention has been attracted to modeling of

the inverse dynamics of MR dampers with the employment of black-box techniques, such as neural networks (Wang & Liao, 2001; Chang & Zhou, 2002; Xia, 2003; Du et al., 2006; Cao et al., 2008), neuro-fuzzy methods (Schurter & Roschke, 2001) and fuzzy logic methods (Zhou et al., 2003; Du & Zhang, 2008).

This chapter describes configuration, fabrication as well as calibration and performance tests of the devised self-sensing MR damper firstly. Then, a black-box identification approach for modeling the forward and inverse dynamics of the self-sensing MR damper is presented, which is developed with the synthesis of NARX model and neural network within a Bayesian inference framework to have the ability of enhancing generalization.

## 2. Self-sensing MR damper

As illustrated in Fig. 1, the configuration of a self-sensing MR damper is composed of damper and sensor parts. The damper part originates from an actuation-only MR damper. It comprises a cylinder with MR fluid, an electromagnet, a diaphragm, an accumulator and a piston housed inside, as well as a pair of electrical wires extended from the electromagnet and through the piston. The body diameter of the damper is 41 mm. It is 208 mm and 155 mm long in fully extended and compressed positions, respectively, and hence can provide a stroke of  $\pm 25$  mm. The magnetic field inside the device can be varied externally by monitoring the input current supplied to the device. The maximum input currents are 1 A and 2 A for continuous and intermittent working situations, respectively.

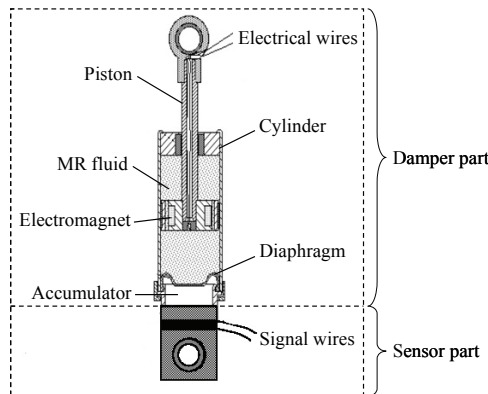


Fig. 1. Schematic diagram of self-sensing MR damper

The sensor part is essentially a prestress-type piezoelectric force sensor attached axially to the damper part, the detailed configuration of which is shown in Fig. 2. Components of the piezoelectric force sensor include a piezoelectric wafer, two electrode wafers, two insulating wafers, two adaptors, a pair of signal wires and a threaded bolt. A lead zirconate titanate (PZT) piezoceramic ring (Ferroperm Pz28), having an outer diameter of 38 mm, an inner diameter of 13 mm and a thickness of 2 mm, is selected as the piezoelectric wafer. Fired silver layers are coated on the two surfaces of the piezoelectric wafer perpendicular to its thickness, and electric polarization is induced along the thickness direction using these electrode surfaces. The electrode wafers are made of a beryllium-copper (Be-Cu) alloy sheet and positioned on either side of the piezoelectric wafer to provide external connections with

the sensor signal wires. The insulating wafers made of polyimide are also in a ring shape with an outer diameter of 40 mm, an inner diameter of 10 mm and a thickness of 0.1 mm. Each of them is inserted between the electrode wafer and the metal adaptor to prevent short-circuiting of the piezoelectric wafer and the whole sensor. These sensor components are sandwiched centrally in a stack between two steel adaptors and assembled by using a standard M10 threaded bolt according to the arrangement in Fig. 2. The bolt is insulated using a plastic band from the electrode wafers and the piezoelectric wafer.

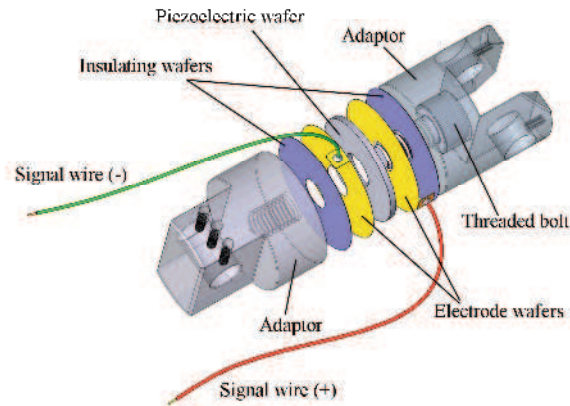


Fig. 2. Assembly diagram of piezoelectric force sensor

Since the piezoelectric force sensor works properly only under compression, the technique of mechanical prestressing is performed on the sensor so that tension forces can be measured while the piezoelectric element remains in compression during operation. A torque driver (BRITTOOL), calibrated with the compression stress of 18 MPa on the piezoelectric wafer for a torque of 30 N·m, is employed to exert torque slowly to the bolt until it is overloaded. During the prestressing, the positive and negative electrodes are connected to form a short-circuit condition to avoid accumulation of charges on the surfaces of the piezoelectric wafer. The assembled sensor is evaluated (to be reported in the next section) and then embedded with the damper part with the configuration of Fig. 1. Fig. 3 shows the photograph of the self-sensing MR damper prototype. In operation, the embedded piezoelectric force sensor senses the variation of force imposed on the damper during structural vibration. The sensed signals are then used to assist in adjusting the current input to the damper through an appropriate control strategy and thereby the commanded damping force. The self-sensing MR damper thus has the dual function of force sensing while controllable damping.



Fig. 3. Photograph of self-sensing MR damper prototype

### 3. Experiments of self-sensing MR damper

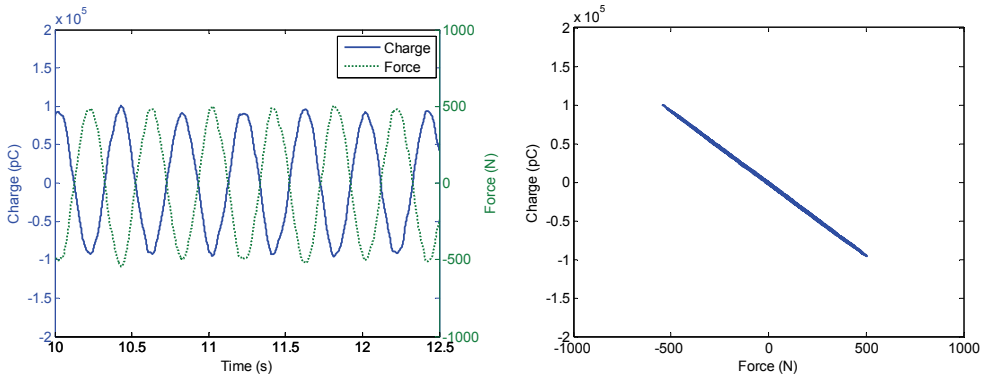
Calibration tests of the piezoelectric force sensor are conducted prior to embedding it with the damper. Then, performance tests are carried out to investigate sensing capability and damping behaviors of the self-sensing MR damper. All the tests are performed on a servohydraulic material testing system (MTS 810). The MTS is operated in force-controlled mode for the calibration tests and in displacement-controlled mode for the performance tests using harmonic excitations with a wide spectrum of frequency and amplitude. The output charge signals generated by the piezoelectric force sensor are measured through a charge meter (Kistler 5015). The charge, force and displacement signals are sampled and recorded by a computer-controlled data acquisition system. The displacement and force excitations exerted to the damper by the MTS are also acquired with the data acquisition unit incorporated in the MTS for further data analysis.

#### 3.1 Calibration

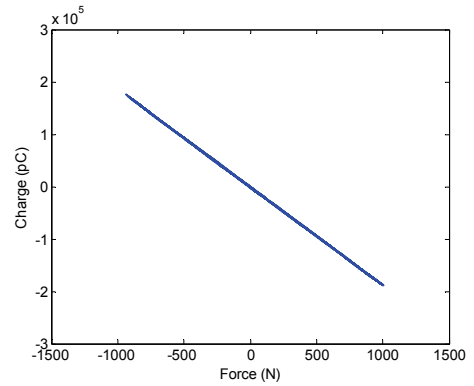
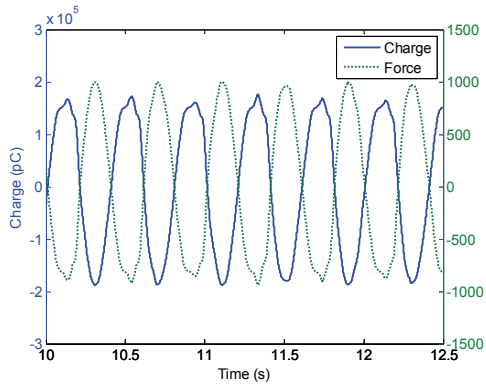
For calibration of the piezoelectric force sensor, force-controlled tests are conducted using sinusoidal excitations with frequencies of 0.5, 1.0, 2.5, 5.0 and 10.0 Hz and amplitudes of 500, 750, 1000, 1250, 1500, 1750 and 2000 N, as well as ramp excitations with frequencies of 0.5, 1.0, 5.0 and 10.0 Hz and amplitudes of 500, 1000, 1500 and 2000 N. Experimental data are used to investigate the relationship between the MTS driving force exerted on the piezoelectric sensor and the output charge from the piezoelectric sensor. Fig. 4 shows the time domain signals of the driving force and the output charge, as well as relationship plots of force versus charge for the selected calibration cases under the sinusoidal force excitations with a frequency of 2.5 Hz and amplitudes of 500 to 2000 N. It is observed that for each case there is always a phase difference of 90° between the output charge and the input force. The relationship between the charge and the force is linear, and the slopes of charge versus force obtained under different excitation conditions are almost identical.

A sensitivity coefficient for the piezoelectric force sensor, quantified as the ratio of charge to force ( $k$ ), can be derived from the linear relationship between the charge ( $Q$ ) and the force ( $F$ ), and is calculated by

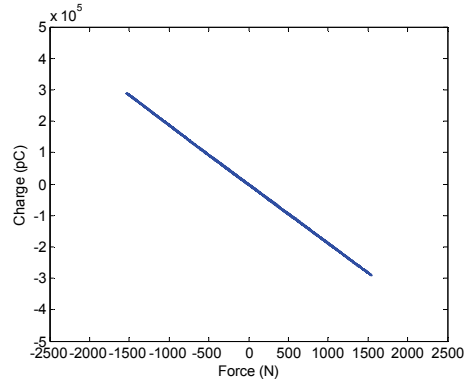
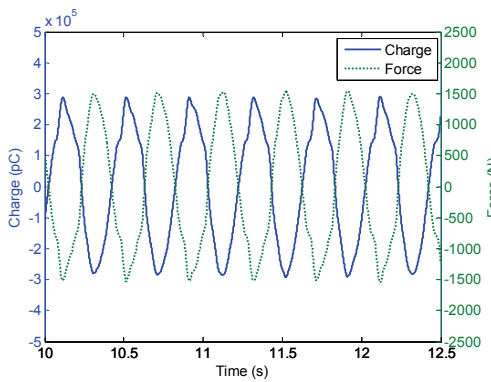
$$k = \frac{\sum_{i=1}^n Q_i^2}{\sum_{i=1}^n (Q_i F_i)} \tag{1}$$



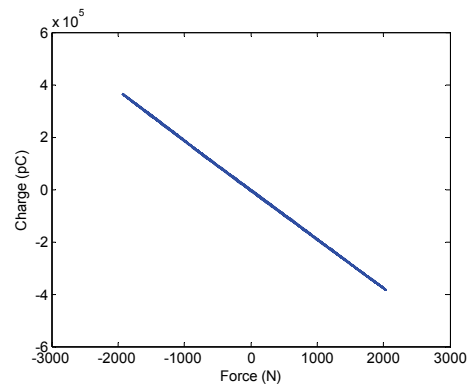
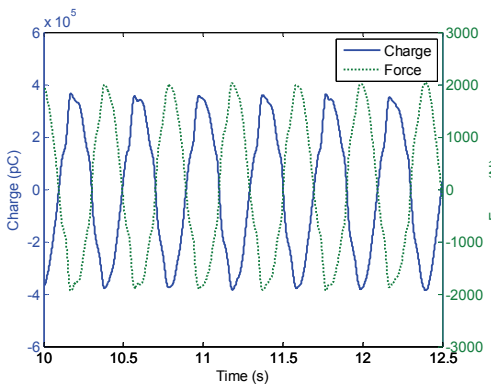
(a) 2.5 Hz, 500 N



(b) 2.5 Hz, 1000 N



(c) 2.5 Hz, 1500 N



(d) 2.5 Hz, 2000 N

Fig. 4. Calibration of piezoelectric force sensor under force-controlled sinusoidal excitations

where  $n$  is the total number of the data samples used for the calibration. In addition, a normalized standard deviation

$$\delta_1 = \sqrt{\frac{1}{n} \sum_{i=1}^n \left( F_i - \frac{Q_i}{k} \right)^2} \bigg/ \sqrt{\frac{1}{n} \sum_{i=1}^n (F_i - \bar{F})^2} \tag{2}$$

is defined to evaluate the accuracy of the sensitivity  $k$ , where  $\bar{F}$  is the mean of the force. The values of the sensitivity coefficient  $k$  and the corresponding normalized standard deviations  $\delta_1$  are calculated for each calibration case (with different combinations of frequencies from 0.5 to 10.0 Hz and excitation amplitudes from 500 to 2000 N). It is found that the sensitivity coefficients obtained from all the calibration cases are almost identical, and the corresponding normalized standard deviations are all less than 0.07. Finally, the sensitivity coefficient for the piezoelectric force sensor is averaged from the results of all the calibration cases to be  $\bar{k} = -187.874 \text{ pC/N}$  with a normalized standard deviation of 0.0102. As a result, the force sensed by the piezoelectric force sensor is expressed as

$$F_{PZT} = Q/\bar{k} \tag{3}$$

**3.2 Performance**

The sensing capability of the self-sensing MR damper is evaluated by the degree of agreement between the force signals from the piezoelectric force sensor and from the MTS transducer, which is defined by a normalized root mean squared residual of

$$\delta_2 = \sqrt{\frac{1}{m} \sum_{j=1}^m (F_{MTS}|_j - F_{PZT}|_j)^2} \bigg/ \sqrt{\frac{1}{m} \sum_{j=1}^m F_{MTS}|_j^2} \tag{4}$$

in which  $m$  is the total number of the data samples used in the calculation. Experimental data are obtained under displacement-controlled excitations of different frequencies and amplitudes and with currents ( $I$ ) supplied to the damper of 0, 0.25, 0.5, 0.75 and 1.0 A, respectively. Fig. 5 shows a comparison of the force signals from the embedded piezoelectric force sensor and from the MTS transducer for the sinusoidal excitation with a frequency of 5 Hz and an amplitude of 5 mm while the input currents are from 0 to 1.0 A, and Table 1 gives the corresponding values of  $\delta_2$ . A good agreement between the two force signals is observed, verifying the good sensing capability of the self-sensing MR damper. Fig. 6 shows force-displacement and force-velocity hysteresis loops of the self-sensing MR damper under displacement-controlled sinusoidal excitations with a frequency of 5 Hz and an amplitude of 5 mm for various currents from 0 to 1.0 A. It is clear that the magnitude of the damper force increases with the increment of the applied current, but the increase slows down when the current approaches to 1.0 A due to the magnetic saturation. Also, the areas enclosed by the force-displacement and force-velocity hysteresis loops enlarge with the increasing current, indicating the enhanced capability of dissipating vibration energy.

Current (A)	0	0.25	0.5	0.75	1.0
$\delta_2$	0.0410	0.0387	0.0396	0.0390	0.0386

Table 1. Normalized root mean squared residuals of force signals

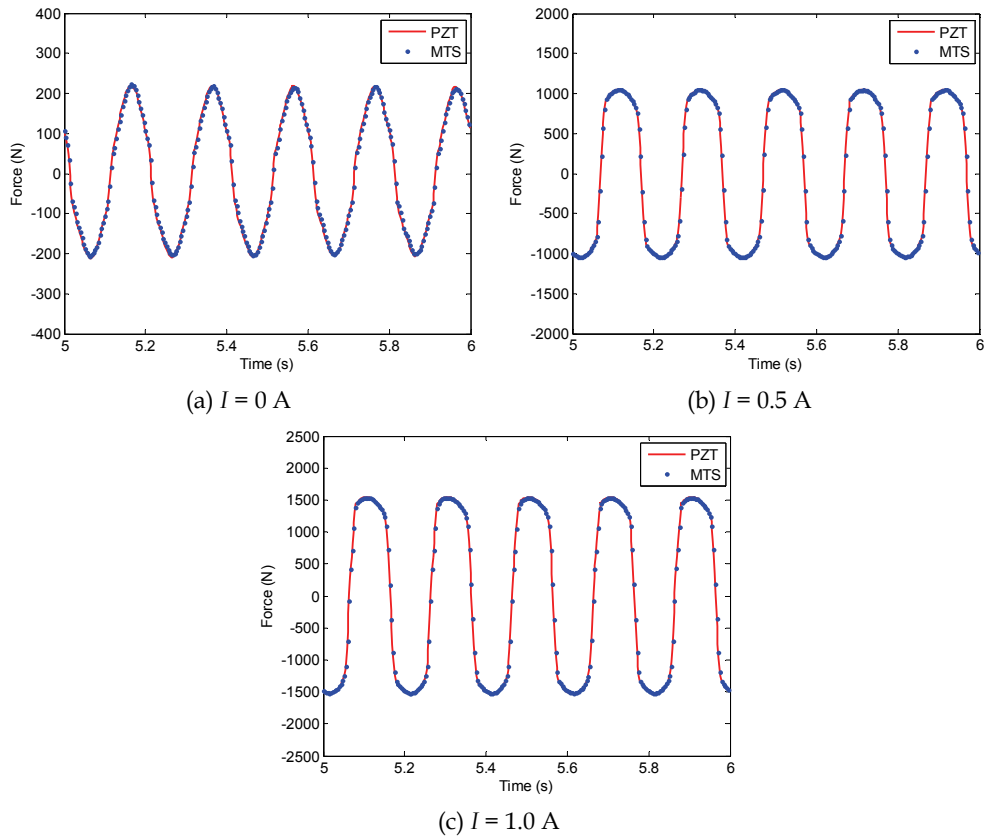


Fig. 5. Comparison between force signals obtained from piezoelectric force sensor and MTS transducer

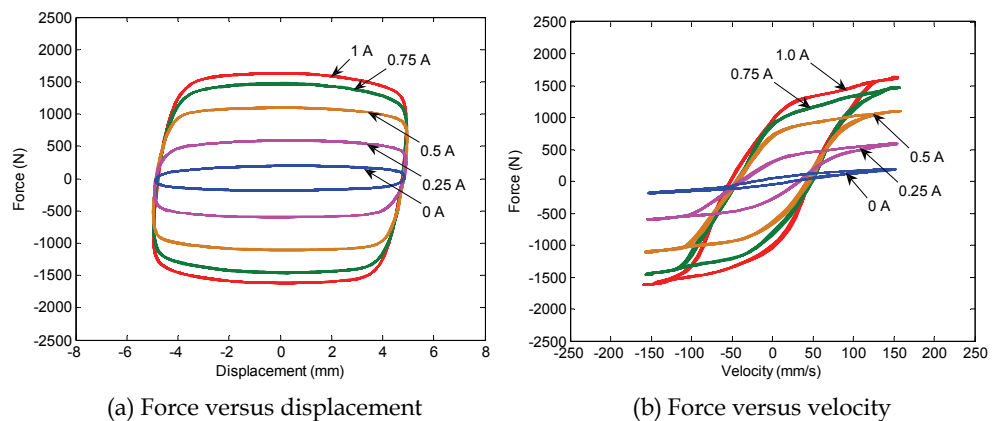


Fig. 6. Hysteresis behavior of self-sensing MR damper

## 4. Modeling of self-sensing MR damper

Due to the inherent nonlinearity of the self-sensing MR damper, the modeling of its dynamics is a nontrivial task. In order to build effective and versatile models for the damper, a black-box modeling method is developed by synthesizing NARX model and neural network from a Bayesian inference perspective.

### 4.1 Methodology

#### 4.1.1 NARX network

NARX model is a very general and powerful black-box model structure due to both its capability of capturing a wide variety of nonlinear dynamic behaviors and the availability of identification algorithms with a reasonable computational cost (Chen et al., 1990). It has been indicated, under mild assumptions, that any finite-dimensional nonlinear system admits an input-output NARX representation, at least locally (Levin & Narendra, 1996). An NARX model is formulated as a discrete time input-output recursive equation of

$$y(t) = f(y(t-1), \dots, y(t-n_y), u(t), u(t-1), \dots, u(t-n_u); \theta) + e(t) \tag{5}$$

where  $u(t)$  and  $y(t)$  denote model input and output variables at time  $t$ ; the integers  $n_u$  and  $n_y$  are the respective maximum lags of the input and the output;  $e(t)$  is the model error between the target and the prediction; and  $f(\cdot, \theta)$  is a nonlinear mapping function of its arguments depending on a vector of parameters  $\theta$ . In order to ensure a good approximation to the real system,  $f(\cdot, \theta)$  should be a universal approximating function.

The multi-layer perceptron (MLP) is an artificial neural network that can realize an overall input-output black-box mapping. It consists of multiple layers of computational neurons interconnected with connection weights in a feedforward way. An MLP with one hidden layer has been theoretically proved to be a universal approximator in the sense that it can approximate any continuous nonlinear function to arbitrary accuracy provided the number of neurons in the hidden layer is adequate and the network weights and biases are adjusted appropriately (Hornik et al., 1989; Leshno et al., 1993). By applying a single-hidden-layer MLP to emulate the multiple-input-single-output NARX model (5), it can be expressed as

$$\hat{y}(t) = g_2 \left( \sum_{j=1}^{n_h} w_j^o g_1 \left( \sum_{i=1}^{n_i} w_{ji}^h z_i(t) + b_j^h \right) + b^o \right) \tag{6}$$

where  $z(t) = [y(t-1), \dots, y(t-n_y), u(t), u(t-1), \dots, u(t-n_u)]$  is the input vector fed into the network;  $z_i$  is the  $i$ th variable of  $z(t)$ ;  $n_i$  ( $= n_y + n_u + 1$ ) denotes the number of input neurons;  $w_{ji}^h$  is the connection weight from the  $i$ th input neuron to the  $j$ th hidden neuron;  $b_j^h$  is the bias for the  $j$ th hidden neuron;  $n_h$  is the total number of hidden neurons;  $w_j^o$  is the weight connecting the only neuron in the output layer to the  $j$ th hidden neuron;  $b^o$  is the bias for the output neuron;  $g_1(\cdot)$  and  $g_2(\cdot)$  are activation functions for the hidden and output layers, respectively;  $\hat{y}(t)$  is the network output at time  $t$ . By expressing the function  $f(\cdot, \theta)$  in Eq. (5) using Eq. (6) with the real valued weights  $w$  ( $= \{w_{ji}^h, w_j^o\}^T$ ) and biases  $b$  ( $= \{b_j^h, b^o\}^T$ ), which together make up the model parameter vector  $\theta$ , the resulting system is named an NARX network. This synthesis results in a powerful model structure that is able to represent complex nonlinear behaviors such as chaos, hysteresis, saturation effects, or combinations of several nonlinear phenomena (Suykens et al., 1996).

### 4.1.2 Bayesian learning

From the statistical point of view, the concept of maximum likelihood, like back-propagation algorithms, is typically employed in the training procedure of MLP models for the parameter estimation. It attempts to search a single set of network parameters from a sequence of training data  $D$  with  $N$  samples through the minimization of an error function, the sum of squares error between the network prediction and the corresponding target

$$E_D = \sum_{t=1}^N (\hat{y}(t) - y(t))^2 \quad (7)$$

However, during such searching (training) process, MLP models based on the maximum likelihood approach are easily led to complex topologies, which may overfit the training data. As a result, such overfitted models will deteriorate the generalization performance and be unable to make predictions as well for unseen input data as for the training case.

One of the feasible procedures to improve generalization is weight decay, which modifies the error function (7) by involving a penalty term to

$$S(\theta) = \beta E_D + \alpha E_\theta \quad (8)$$

where the regularizing term  $E_\theta = \sum_{i=1}^M \theta_i^2$  is the sum of squares of the  $M$  network parameters

(weights and biases), which constrains the complexity of the network by limiting the growth of the network parameters; and  $\alpha$  and  $\beta$  are regularization parameters, which serve to balance the trade-off between the prediction accuracy and the model complexity. MacKay (1992a, b) has made extensive investigations on the application of a Bayesian inference technique to adapt the weights and biases through network training and meanwhile to optimize the regularization parameters in an automated fashion.

Unlike the maximum likelihood approach, the Bayesian inference technique considers a probability distribution over the network parameters, which represents the relative degree of belief in different parameter values and is described by a prior distribution  $P(\theta | \alpha)$  in the absence of any data. Once the data set  $D$  is taken, the posterior probability distribution for the network parameters can be expressed using the Bayes' theorem as

$$P(\theta | D, \alpha, \beta) = \frac{P(D | \theta, \beta) P(\theta | \alpha)}{P(D | \alpha, \beta)} \quad (9)$$

where  $P(D | \theta, \beta)$  is the likelihood of the data that accounts for the network accuracy on the training data; and  $P(D | \alpha, \beta)$  is a normalization factor which ensures that the posterior gives unity when integrated over the parameter space.

By assuming a zero-mean Gaussian noise in the training data  $D$  and Gaussian priors for the network parameters  $\theta$ , the likelihood of the data and the prior probability of the parameters can be written respectively as

$$P(D | \theta, \beta) = \frac{1}{Z_D(\beta)} \exp(-\beta E_D), \quad P(\theta | \alpha) = \frac{1}{Z_\theta(\alpha)} \exp(-\alpha E_\theta) \quad (10a, b)$$

where  $Z_D(\beta) = (\pi/\beta)^{N/2}$  and  $Z_\theta(\alpha) = (\pi/\alpha)^{M/2}$ .

Substitution of Eq. (10) into Eq. (9) obtains the posterior probability distribution as

$$P(\theta | D, \alpha, \beta) = \frac{1}{Z_s(\alpha, \beta)} \exp(-S(\theta)) \tag{11}$$

where  $S(\theta)$  is given by Eq. (8) and  $Z_s(\alpha, \beta) = \int \exp(-S(\theta)) d\theta$ .

Accordingly, the network parameters corresponding to the maximum posterior distribution or the most plausible network parameters  $\theta^{MP}$  can be found by minimizing the negative logarithm of Eq. (11) with respect to the network parameters. Since the normalizing factor  $Z_s(\alpha, \beta)$  is independent of the network parameters, this is equivalent to minimizing the regularized error function  $S(\theta)$  given by Eq. (8). Therefore, by solving the parameter optimization problem to minimize the objective function of Eq. (8), the maximum posterior network parameters can be inferred during the network learning procedure.

The other crucial inference step in the Bayesian learning technique is the optimization of the regularization parameters  $\alpha$  and  $\beta$ . By applying the Bayes' theorem, the posterior probability for these two parameters given the data  $D$  is represented as

$$P(\alpha, \beta | D) = \frac{P(D | \alpha, \beta) P(\alpha, \beta)}{P(D)} \tag{12}$$

The prior  $P(D | \alpha, \beta)$  is assumed to be chosen as very insensitive to the values of  $\alpha$  and  $\beta$ . Since  $P(D)$  is independent of  $\alpha$  and  $\beta$ , the maximum posterior values for the regularization parameters are found by maximizing the likelihood term  $P(D | \alpha, \beta)$ , which is the normalization factor in Eq. (9). Using Eqs. (9) to (11), the likelihood is derived as

$$P(D | \alpha, \beta) = \frac{P(D | \theta, \beta) P(\theta | \alpha)}{P(\theta | D, \alpha, \beta)} = \frac{Z_s(\alpha, \beta)}{Z_D(\beta) Z_\theta(\alpha)} \tag{13}$$

If the Gaussian approximation is made for the posterior distribution of the network parameters, then  $Z_s$  is given by (MacKay, 1992a)

$$Z_s \approx (2\pi)^{M/2} |H^{MP}|^{-1/2} \exp(-S(\theta^{MP})) \tag{14}$$

where  $H^{MP}$  is the Hessian matrix  $H$  of the regularized objective function  $S(\theta)$  evaluated at  $\theta^{MP}$ . Introducing Eq. (14) into Eq. (13) and taking the derivatives of the logarithm of the likelihood respectively with respect to  $\alpha$  and  $\beta$  yield

$$\alpha^{MP} = \frac{\gamma}{2E_\theta^{MP}}, \quad \beta^{MP} = \frac{N - \gamma}{2E_D^{MP}} \tag{15a, b}$$

where  $\gamma = M - 2\alpha^{MP} \text{trace}((H^{MP})^{-1})$  measures the number of network parameters that are effectively involved in reducing the objective function.

In this study, the Levenberg-Marquardt (LM) algorithm (Marquardt, 1963; Hagan and Menhaj, 1994) is employed to find the most plausible network parameters  $\theta^{MP}$  to minimize the objective function Eq. (8), due to its efficient and stable convergence for moderate-sized neural networks that contain up to a few hundred weights. The costly computation of the

Hessian matrix can also be solved by making a Gauss-Newton approximation to it using the LM algorithm. As  $\gamma$  depends on  $\alpha$ , the values of  $\alpha$  and  $\beta$  are re-estimated iteratively using Eq. (15), which is carried out during the training process.

In practical implementation of the Bayesian learning technique, it is suggested that all data sets be normalized into the range of  $[-1, 1]$  to avoid that some network parameters will be trained to be extremely large or small to accommodate different scales of input and target variables. In addition, the procedure of multiple random initializations of network parameters is used to retrain the network to assure that the optimal solution, instead of local minima, has been reached.

## 4.2 Forward dynamic model

### 4.2.1 Model formulation

In terms of Eq. (5), an NARX network model for describing the forward dynamics of the devised self-sensing MR damper can be expressed as

$$\hat{F}(t) = \mathcal{N}_{fwd}(x(t), \dots, x(t-n_x), \dot{x}(t), \dots, \dot{x}(t-n_{\dot{x}}), I(t), \dots, I(t-n_I), F(t-1), \dots, F(t-n_F)) \quad (16)$$

where  $x$ ,  $\dot{x}$ ,  $I$  and  $F$  are displacement, velocity of the damper piston, current input and damper force, respectively;  $n_x$ ,  $n_{\dot{x}}$ ,  $n_I$  and  $n_F$  denote the respective maximum lags of the displacement, velocity, current and damper force; and  $\mathcal{N}_{fwd}(\cdot)$  represents the forward input-output mapping identified by an MLP. In Eq. (16), present and past values of the piston displacement, velocity, current together with past values of the sensed damper force, which contain dynamic physical information of the damper, are chosen as possible network input variables to describe its forward dynamics and predict the one-step-ahead damper force.

To assess the prediction performance of the formulated NARX network model, the root mean square error (RMSE) between the measured damper force and the prediction from the model is adopted and evaluated, which is given by

$$\text{RMSE} = \sqrt{\frac{1}{T} \sum_{t=1}^T [F(t) - \hat{F}(t)]^2} \quad (17)$$

### 4.2.2 Model architecture design

The NARX network employed in this study is configured to consist of three successive layers, which are an input layer, a hidden layer and an output layer, and is formulated as Eq. (6). The activation functions for the hidden and output layers are chosen as a hyperbolic tangent sigmoid function and a linear function, respectively, and expressed as

$$g_1(a) = \tanh(a) = \frac{1 - e^{-2a}}{1 + e^{-2a}}, \quad g_2(a) = a \quad (18a, b)$$

The experimental data from the displacement-controlled tests are used to train, design and evaluate the NARX network model for the self-sensing MR damper. The modeling process is divided into two stages. In the first stage, a training set and a validation set are built up with the acquired experimental data. The training set is used to adapt the network parameters through the Bayesian learning, while the validation set is used for designing

model architecture. In the second stage, the well-trained model is evaluated using a novel test set uninvolved in the first stage to examine its generalization performance. Table 2 lists information of different sinusoidal excitations and input current levels for generating the training, validation and test sets.

Data set	Sinusoidal excitation		Current
	Amplitude	Frequency	
Training	1 mm	1 Hz	0:0.25:1.0 A
	5 mm	5 Hz	0:0.25:1.0 A
	1 mm	5 Hz	0:0.5:1.0 A
	5 mm	1 Hz	0:0.5:1.0 A
Validation	1 mm	1 Hz	0.5 A
	5 mm	5 Hz	0.5 A
	1 mm	5 Hz	0.25, 0.75 A
	5 mm	1 Hz	0.25, 0.75 A
Test	5 mm	2.5 Hz	0:0.25:1.0 A

Table 2. Experimental cases for generation of training, validation and test sets

In designing the NARX network architecture, three important issues are addressed with the purpose of realizing superior modeling performance and enhancing generalization capability. These issues include selection of an optimal combination of input variables, choice of the required numbers of input lags and determination of the optimal number of neurons in the hidden layer.

From the physical behaviors of the self-sensing MR damper shown in Fig. 6 and the model formulation (16), the damper piston displacement ( $x$ ) and velocity ( $\dot{x}$ ), the current input to the damper ( $I$ ), and the past values of the damper force ( $F$ ) can be chosen as the NARX network inputs. However, to reduce redundant information and obtain a simple network topology for improving model performance, the optimal combination of input variables is identified for the NARX network. In terms of the RMSE index in Eq. (17) evaluated on the validation set in Table 2, Fig. 7 compares the model performance with different input combinations among the input variables  $x$ ,  $\dot{x}$ ,  $I$  and  $F$ . Here the input lags  $n_x = n_{\dot{x}} = n_I = 0$  and  $n_F = 1$  are taken and the number of hidden neurons ( $n_h$ ) is equally set to be 15 for each network configuration. It evidences from Fig. 7 that as the combination of either ( $x$ ,  $I$ ,  $F$ ) or ( $x$ ,  $\dot{x}$ ,  $I$ ) is used, poor model performance is obtained, which reveals that the use of both the velocity  $\dot{x}$  and the past damper force  $F$  is important and essential for enhancing the model prediction quality. The involvement of the current  $I$  is also necessary in that it affects the damper force significantly, which is verified by comparing the results with the inputs of ( $x$ ,  $\dot{x}$ ,  $F$ ) and ( $x$ ,  $\dot{x}$ ,  $I$ ,  $F$ ). Moreover, if all the three variables of  $\dot{x}$ ,  $I$  and  $F$  are taken, the role played by the displacement  $x$  is negligible.

Fig. 8 shows the network performance over various input combinations, numbers of input lags ( $n_x = n_{\dot{x}} = n_I = n_F = 1, 2, 3$ ) and numbers of hidden neurons ( $n_h = 5, 10, 15, 20$ ). By further comparing the results on different input combinations in Fig. 8, the significance of involving  $\dot{x}$ ,  $I$  and  $F$  into the network inputs is again confirmed. The RMSE values of the combination ( $\dot{x}$ ,  $I$ ,  $F$ ) are comparable to those of the combination ( $x$ ,  $\dot{x}$ ,  $I$ ,  $F$ ) in the same case of input lag. Thereby, from the view of model simplicity, the velocity  $\dot{x}$ , the current  $I$  and the past damper force  $F$  are finally selected as the input variables for the forward model.

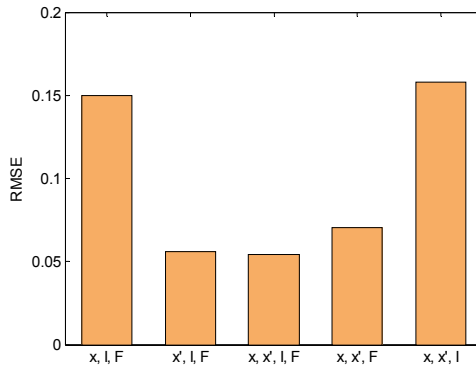


Fig. 7. RMSE analysis for different input combinations ( $n_x = n_{\dot{x}} = n_I = 0, n_F = 1, n_h = 15$ )

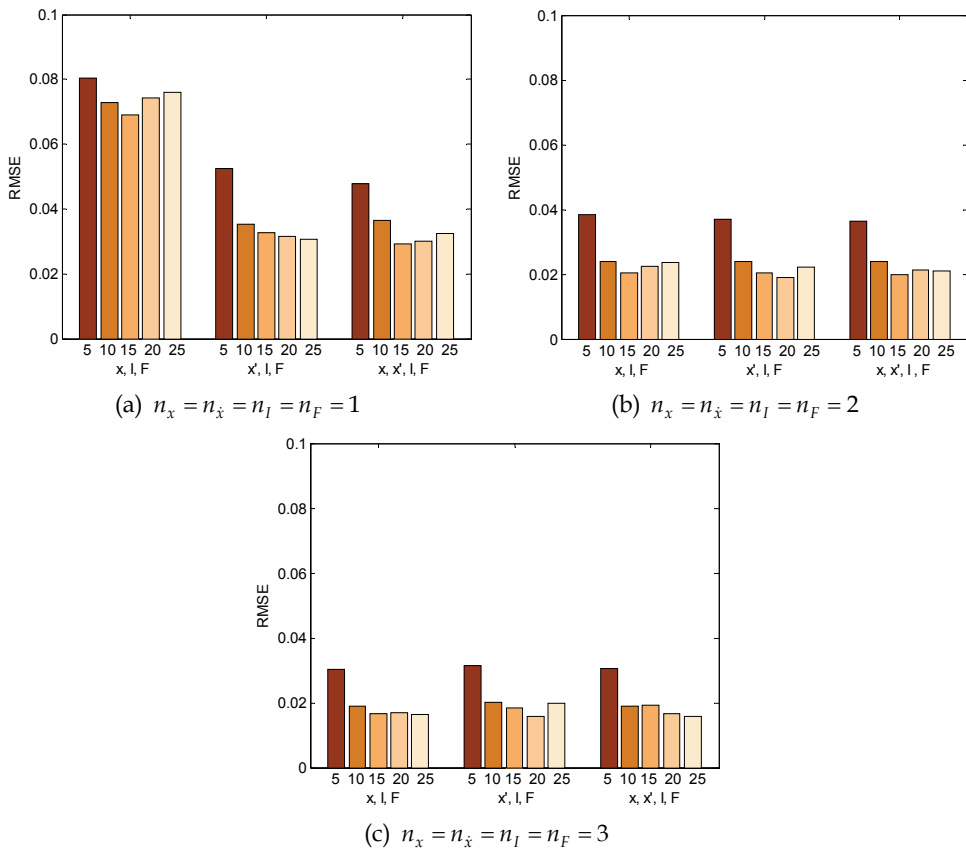


Fig. 8. RMSE analysis for different input lags

On the other hand, effects of the input lags can be observed from Figs. 7 and 8. The RMSE of validation for each network configuration decrease with the increment of the input lag. The

rate of decrease becomes less as larger input lag is used. Especially, for models with inputs of  $(\dot{x}, I, F)$  and enough hidden neuron number, larger input lags ( $n_x = n_{\dot{x}} = n_I = n_F = 3$ ) has a relatively small effect on further enhancing the model performance in comparison with the case of  $n_x = n_{\dot{x}} = n_I = n_F = 2$ . Consequently, the input lag for each input variable is chosen to be two to achieve a compact network topology and its resulting training efficiency.

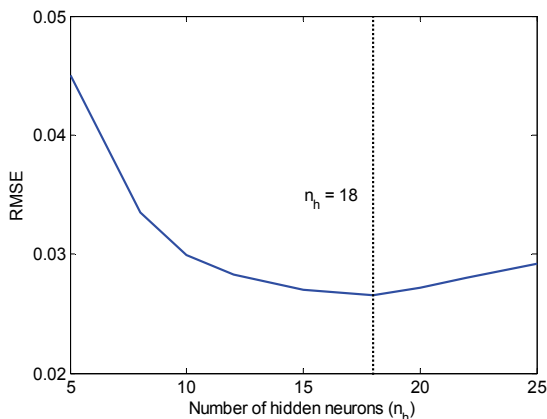


Fig. 9. RMSE analysis for different numbers of hidden neurons ( $n_x = n_{\dot{x}} = n_I = n_F = 2$ )

Once the input variables and the number of input lags are determined, it is simple to decide the number of hidden neurons ( $n_h$ ) using a trial and error procedure by extending it from 5 to 25. Fig. 9 displays the RMSE index (evaluated on the validation set) as a function of the number of hidden neurons ( $n_h$ ). The optimal number of hidden neurons is determined to be 18, in which the minimal RMSE of validation is reached.

With a comprehensive consideration of topology simplicity and model accuracy, an NARX network, configured with 8 input neurons, 18 neurons in one-hidden-layer and 1 output neuron, is designed for modeling the forward dynamics of the self-sensing MR damper.

#### 4.2.3 Model prediction capability under harmonic excitations

Generalization performance of the configured Bayesian NARX network is examined using the test set given in Table 2. The test set is acquired under 2.5 Hz sinusoidal displacement excitations with an amplitude of 5 mm and current inputs ranging from 0 A to 1.0 A, which has not been involved in the stage of training and is new for the model assessment. The one-step-ahead damper force is produced from the model once it is exposed to the test data. The RMSE between the predicted and measured damper forces is less than 0.04 for each case of input current in the test set, as shown in Table 3, which demonstrates that the model generalizes well. Fig. 10 plots the hysteresis loops of force-displacement and force-velocity of the damper obtained from the predicted results of the model and from the experimentally recorded data. A comparison between the predicted and measured results indicates that the NARX network model accurately describes the hysteretic behaviors of the self-sensing MR damper. It also well learns the saturation effects of the damper, verifying the learning ability of the Bayesian NARX network technique.

Current (A)	0	0.25	0.5	0.75	1.0
RMSE	0.0269	0.0132	0.0173	0.0238	0.0312

Table 3. RMSE results for test set

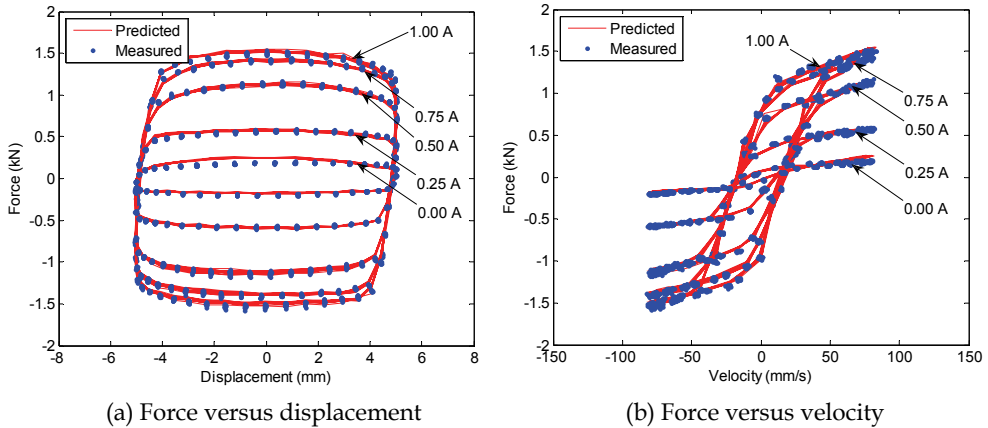


Fig. 10. Comparison of predicted and measured force-displacement and force-velocity loops under 5 mm, 2.5 Hz harmonic excitation

#### 4.2.4 Model prediction capability under random excitations

All of the data examined previously for the Bayesian NARX network modeling have been based on the responses of the self-sensing MR damper subjected to harmonic displacement-controlled excitations and commanded by currents held at constant levels. However, an important requirement for system modeling is a set of representative data containing abundant system information. To ensure generalization and robustness of the damper models in practical control circumstances, multiple harmonic excitations are often insufficient due to the limited amount of information included within them. Therefore, random displacement-controlled excitations and current inputs are more appropriate for activating the dynamic behaviors of the self-sensing MR damper and acquiring the random data for training the NARX network models. In this subsection, performance of the Bayesian NARX network model with random excitations and input commands will be examined.

For acquiring random responses, the self-sensing MR damper is installed with a steel-frame structure mounted on a shaking table, as shown in Fig. 11. The structure consists of a stack of steel plates weighing 655.8 kg as the floor mass and four steel columns with 75 mm × 10 mm rectangular cross-sections. The damper is connected between the mass and a support in the height of 745 mm. The support for fixing one end of the damper is designed to be rigid enough to assume this end is unmovable. The structural system is excited by band-limited white noise ground motions produced by the shaking table, while the damper is controlled by varying current commands. The real-time data acquisition for a variety of structural responses, which include ground acceleration, floor displacement, damper piston displacement, current and damper force, is accomplished by a dSPACE system by setting the sampling rate to be 250 Hz. Velocity of the damper piston is calculated from the measured piston displacement using a finite difference approximation.

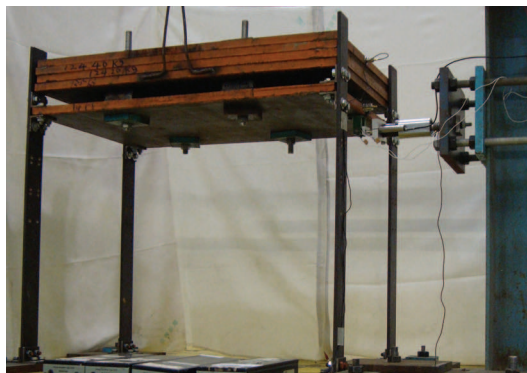


Fig. 11. Experimental setup for random vibration testing of self-sensing MR damper

With the purpose of assessing its prediction capability under random loadings, the previous optimal Bayesian NARX network model is retrained using the random response data of the self-sensing MR damper, which are acquired when the structural system subjected to narrow-band white noise excitations with amplitude of about  $8 \text{ m/s}^2$  and frequency within  $0.8\text{-}10 \text{ Hz}$ . The damper is controlled by random current with amplitude ranging from  $0 \text{ A}$  to  $1.85 \text{ A}$  and frequency within  $0\text{-}10 \text{ Hz}$ . Fig. 12 illustrates the damper piston velocity, current and damper force signals for network training within a time window of  $10 \text{ s}$ . After training, another three sets of measured data unseen during the training phase are used for verification of the trained model. As listed in Table 4, these test sets are obtained when the structure is excited by ground motions with different frequency and amplitude ranges, while the damper is prescribed with three types of currents, including constant current held at  $0.97 \text{ A}$ , chirp current with amplitude between  $0\text{-}1.85 \text{ A}$  and frequency range of  $0.1\text{-}10 \text{ Hz}$ , as well as random current with amplitude between  $0\text{-}1.85 \text{ A}$  and frequency within  $0\text{-}5 \text{ Hz}$ . Fig. 13 shows time histories of the damper forces predicted by the Bayesian NARX network model based on the test sets shown in Table 4 together with the measured damper forces, in which the prediction residuals are also superposed. Through comparisons, the forward

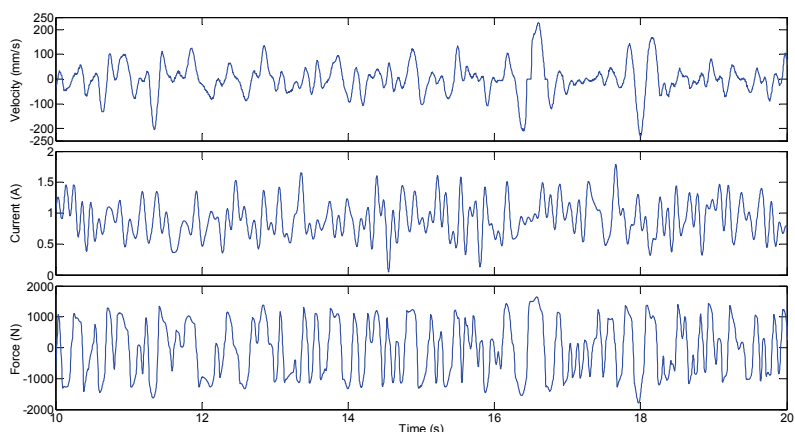


Fig. 12. Random signals for network training

Data set	Ground acceleration excitation		Current		
	Amplitude	Frequency	Type	Amplitude	Frequency
Training	-7.7~8.1 m/s <sup>2</sup>	0.8-10 Hz	Random	0-1.85 A	0-10 Hz
Test I	-5.6~5.9 m/s <sup>2</sup>	0.8-5 Hz	Constant	0.97 A	--
Test II	-5.3~5.2 m/s <sup>2</sup>	0.5-10 Hz	Chirp	0-1.85 A	0.1-10 Hz
Test III	-8.2~8.0 m/s <sup>2</sup>	0.5-10 Hz	Random	0-1.85 A	0-5 Hz

Table 4. Information of excitations for generation of training and test sets

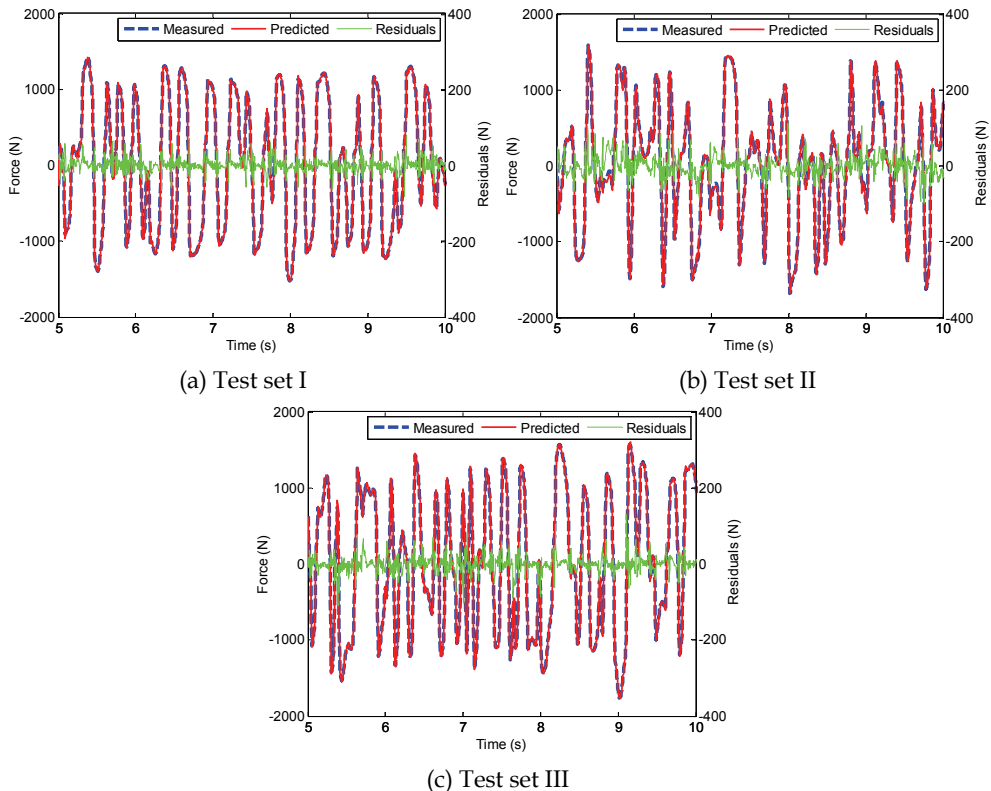


Fig. 13. Comparison between predicted and measured damper forces and their residuals

model effectively predicts the damper forces with the RMSE values of 19.20 N, 27.30 N and 23.01 N for test sets I, II and III, respectively, which are all lower than 5% of the norm values of their corresponding target forces. Hence, the Bayesian NARX network model generalizes well to the random situations.

### 4.3 Inverse dynamic model

In control application of the self-sensing MR damper, similar to the conventional MR dampers, current is the only physical quantity that can be directly controlled to render the

damper to track the optimal control force calculated by a certain active control algorithm. Dyke et al. (1996) proposed a clipped optimal control algorithm for commanding the current or voltage which, however, only switches at either the minimum or the maximum achievable level. To avoid the damper working in such a bang-bang manner, which requires very fast dynamic responses of a current driver and the damper, it is beneficial and essential to develop an inverse dynamic model for the self-sensing MR damper to produce continuously varying current signals. However, it is still a difficult task to build such an inverse model for the highly nonlinear damper. Due to the success of the Bayesian NARX network in modeling the forward dynamics of the self-sensing MR damper, the feasibility of applying this technique to emulate the inverse dynamics of the self-sensing MR damper is explored.

According to Eqs. (5) and (16), an NARX network model for the inverse dynamics of the self-sensing MR damper can be represented as

$$\hat{I}(t) = \mathcal{N}_{inv}(x(t), \dots, x(t-n_x), \dot{x}(t), \dots, \dot{x}(t-n_{\dot{x}}), F(t), \dots, F(t-n_F), I(t-1), \dots, I(t-n_I)) \quad (19)$$

where  $\mathcal{N}_{inv}(\cdot)$  denotes an MLP trained to approximate the inverse input-output relationship of the damper. Present and past values of the damper piston displacement, velocity and the desired damper force together with past values of the applied current are taken as possible input variables for the inverse model to decide the required current  $\hat{I}(t)$  for the damper to produce the instant value of the desired control force  $F(t)$ .

Similar to the forward model, the input variables for the inverse model are also determined to be the damper piston velocity  $\dot{x}$ , the desired damper force  $F$  and the past current  $I$  with input lags of  $n_{\dot{x}} = n_F = n_I = 2$ . The network structure is the same as Eq. (6), and consists of three sequential layers assigned with 8 input neurons, 18 hidden neurons and 1 output neuron, respectively. Transfer functions for the hidden layer and the output layer are taken as a hyperbolic tangent sigmoid function and a linear function, respectively, in the forms given by Eq. (18).

The envisaged inverse NARX network model is then trained by employing the Bayesian learning algorithm. The training data are the same as the random signals employed for building the forward model, as shown in Fig. 12 and Table 4. Subsequently, test sets defined in Table 4 are presented to the inverse model to evaluate the prediction performance. Fig. 14 illustrates the predicted currents from the well trained Bayesian NARX network model in comparison with the measured ones, as well as their residuals. It is seen that the predicted currents in the constant, chirp and random cases agree well with the measured currents applied to the damper. The RMSE values of predictions for test sets I, II and III are 0.016, 0.018 and 0.008 A, respectively. These verification results demonstrate that the developed Bayesian NARX network model satisfactorily emulates the inverse dynamics of the self-sensing MR damper and is adequate for control applications.

## 5. Conclusions

A self-sensing MR damper with embedded piezoelectric force sensor was devised, calibrated and characterized. Experimental results have shown reliable force sensing and controllable damping capabilities, as well as nonlinear hysteresis and saturation behaviors of the self-sensing MR damper. The attractive sensing-while-damping function renders the

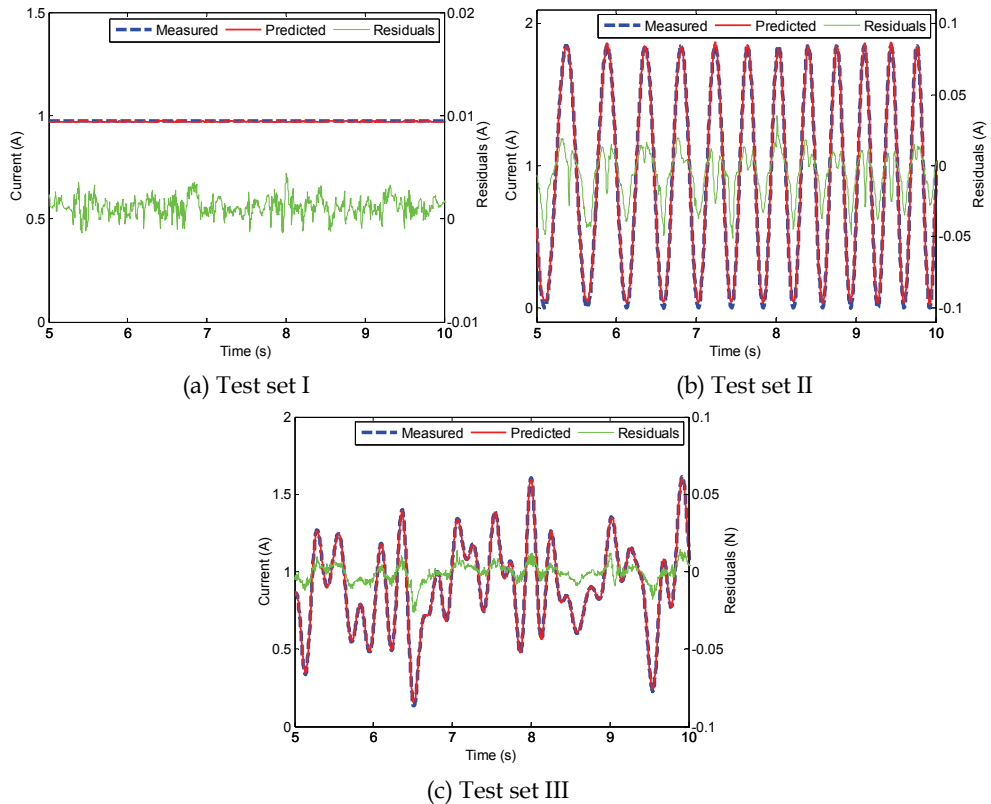


Fig. 14. Comparison between predicted and measured currents and their residuals

devised damper promising for real-time closed-loop control of structural vibration in a relatively simple and cost-effective manner.

In order to formulate the inherently nonlinear dynamics of the self-sensing MR damper for its control application, a black-box modeling method has been developed by synthesizing NARX model and neural network within a Bayesian inference framework. Verification results based on experimental data have demonstrated that the formulated Bayesian NARX network models with an appropriate architecture can accurately emulate the forward and inverse dynamic behaviors of the self-sensing MR damper. Also, they exhibit good generalization capability when exposed to different test scenarios, due to the effect of the automated regularization of the Bayesian learning technique during the training phase. As a result, the developed models can be further integrated with semiactive control algorithms to achieve real-time structural vibration control using the self-sensing MR damper.

## 6. Acknowledgements

The work described in this chapter was supported in part by a grant from the Research Grants Council of the Hong Kong Special Administrative Region, China (Project No. PolyU 5252/07E), and partially by a grant from The Hong Kong Polytechnic University through

the Development of Niche Areas Programme (Project No. 1-BB95). These supports are gratefully acknowledged.

## 7. References

- Cao, M.; Wang, K. W. & Lee, K. Y. (2008). Scalable and invertible PMNN model for magneto-rheological fluid dampers. *Journal of Vibration and Control*, Vol. 14, No. 5, (May 2008) 731-751, ISSN 1077-5463
- Carlson, J. D.; Catanzarite, D. M. & Clair, K. A. St. (1996). Commercial magneto-rheological fluid devices. *International Journal of Modern Physics B*, Vol. 10, No. 23-24, (October 1996) 2857-2865, ISSN 0217-9792
- Chang, C.-C. & Roschke, P. N. (1998). Neural network modeling of a magnetorheological damper. *Journal of Intelligent Material Systems and Structures*, Vol. 9, No. 9, (September 1998) 755-764, ISSN 1045-389X
- Chang, C.-C. & Zhou, L. (2002). Neural network emulation of inverse dynamics for a magnetorheological damper. *Journal of Structural Engineering*, Vol. 128, No. 2, (February 2002) 231-239, ISSN 0733-9445
- Chen, S.; Billings, S. A. & Grant, P. M. (1990). Non-linear system identification using neural networks. *International Journal of Control*, Vol. 51, No. 6, (January 1990) 1191-1214, ISSN 0020-7179
- Chen, Z. Q.; Wang, X. Y.; Ko, J. M.; Ni, Y. Q.; Spencer, B. F.; Yang, G. & Hu, J. H. (2004). MR damping system for mitigating wind-rain induced vibration on Dongting Lake Cable-Stayed Bridge. *Wind and Structures*, Vol. 7, No. 5, (September 2004) 293-304, ISSN 1226-6116
- Choi, S.-B.; Seong, M.-S. & Ha, S.-H. (2009). Vibration control of an MR vehicle suspension system considering both hysteretic behavior and parameter variation. *Smart Materials and Structures*, Vol. 18, No. 12, (December 2009) 125010, ISSN 0964-1726
- Du, H.; Lam, J. & Zhang, N. (2006). Modelling of a magneto-rheological damper by evolving radial basis function networks. *Engineering Applications of Artificial Intelligence*, Vol. 19, No. 8, (December 2006) 869-881, ISSN 0952-1976
- Du, H. & Zhang, N. (2008). Application of evolving Takagi-Sugeno fuzzy model to nonlinear system identification. *Applied Soft Computing*, Vol. 8, No. 1, (January 2008) 676-686, ISSN 1568-4946
- Duan, Y. F.; Ni, Y. Q. & Ko, J. M. (2005). State-derivative feedback control of cable vibration using semiactive magnetorheological dampers. *Computer-Aided Civil and Infrastructure Engineering*, Vol. 20, No. 6, (November 2005) 431-449, ISSN 1093-9687
- Dyke, S. J.; Spencer, B. F. Jr.; Sain, M. K. & Carlson, J. D. (1996). Modeling and control of magnetorheological dampers for seismic response reduction. *Smart Materials and Structures*, Vol. 5, No. 5, (October 1996) 565-575, ISSN 0964-1726
- Gandhi, F.; Wang, K. W. & Xia, L. (2001). Magnetorheological fluid damper feedback linearization control for helicopter rotor application. *Smart Materials and Structures*, Vol. 10, No. 1, (February 2001) 96-103, ISSN 0964-1726
- Gordaninejad, F.; Saiidi, M.; Hansen, B. C.; Ericksen, E. O. & Chang, F.-K. (2002). Magneto-rheological fluid dampers for control of bridges. *Journal of Intelligent Material Systems and Structures*, Vol. 13, No. 2-3, (February 2002) 167-180, ISSN 1045-389X

- Hagan, M. T. & Menhaj, M. B. (1994). Training feedforward networks with the Marquardt algorithm. *IEEE Transactions on Neural Networks*, Vol. 5, No. 6, (November 1994) 989-993, ISSN 1045-9227
- Hornik, K.; Stinchcombe, M. & White, H. (1989). Multilayer feedforward networks are universal approximators. *Neural Networks*, Vol. 2, No. 5, (July 1989) 359-366, ISSN 0893-6080
- Hu, W. & Wereley, N. M. (2008). Hybrid magnetorheological fluid-elastomeric lag dampers for helicopter stability augmentation. *Smart Materials and Structures*, Vol. 17, No. 4, (August 2008) 045021, ISSN 0964-1726
- Ikhouane, F. & Dyke S. J. (2007). Modeling and identification of a shear mode magnetorheological damper. *Smart Materials and Structures*, Vol. 16, No. 3, (June 2007) 605-616, ISSN 0964-1726
- Jiménez, R. & Álvarez-Icaza, L. (2005). LuGre friction model for a magnetorheological damper. *Structural Control and Health Monitoring*, Vol. 12, No. 1, (October 2004) 91-116, ISSN 1545-2255
- Jin, G.; Sain, M. K. & Spencer, B. F. Jr. (2005). Nonlinear blackbox modeling of MR-dampers for civil structural control. *IEEE Transactions on Control Systems Technology*, Vol. 13, No. 3, (May 2005) 345-355, ISSN 1063-6536
- Johnson, E. A.; Baker, G. A.; Spencer, B. F. Jr. & Fujino, Y. (2000). Mitigating stay cable oscillation using semiactive damping, *Proceedings of SPIE, Smart Structures and Materials 2000: Smart Systems for Bridges, Structures, and Highways*, Vol. 3988, pp. 207-216, ISBN 0-8194-3606-2, Newport Beach, CA, USA, March 2000, SPIE, Bellingham
- Jung, H.-J.; Spencer, B. F. Jr.; Ni, Y. Q. & Lee, I.-W. (2004). State-of-the-art of semiactive control systems using MR fluid dampers in civil engineering applications. *Structural Engineering and Mechanics*, Vol. 17, No. 3, (March 2004) 493-526, ISSN 1225-4568
- Kamath, G. M. & Wereley, N. M. (1997). A nonlinear viscoelastic-plastic model for electrorheological fluids. *Smart Materials and Structures*, Vol. 6, No. 3, (June 1997) 351-359, ISSN 0964-1726
- Ko, J. M.; Ni, Y. Q.; Chen, Z. Q. & Spencer, B. F. Jr. (2002). Implementation of magnetorheological dampers to Dongting Lake Bridge for cable vibration mitigation, *Proceedings of the Third World Conference on Structural Control*, Vol. 3, pp. 777-786, ISBN 0-4744-8980-8, Como, Italy, April 2002, John Wiley & Sons, Chichester
- Leshno, M.; Lin, V. Y.; Pinkus, A. & Schocken, S. (1993). Multilayer feedforward networks with a nonpolynomial activation function can approximate any function. *Neural Networks*, Vol. 6, No. 6, (August 1993) 861-867, ISSN 0893-6080
- Leva, A. & Piroddi, L. (2002). NARX-based technique for the modelling of magnetorheological damping devices. *Smart Materials and Structures*, Vol. 11, No. 1, (February 2002) 79-88, ISSN 0964-1726
- Levin, A. U. & Narendra, K. S. (1996). Control of nonlinear dynamical systems using neural networks - part II: observability, identification, and control. *IEEE Transactions on Neural Networks*, Vol. 7, No. 1, (January 1996) 30-42, ISSN 1045-9227
- Li, H.; Liu, M.; Li, J.; Guan, X. & Ou, J. (2007). Vibration control of stay cables of the Shandong Binzhou Yellow River Highway Bridge using magnetorheological fluid

- dampers. *Journal of Bridge Engineering*, Vol. 12, No. 4, (July/August 2007) 401-409, ISSN 1084-0702
- Liao, W. H. & Wang, D. H. (2003). Semiactive vibration control of train suspension systems via magnetorheological dampers. *Journal of Intelligent Material Systems and Structures*, Vol. 14, No. 3, (March 2003) 161-172, ISSN 1045-389X
- Loh, C.-H.; Lynch, J. P.; Lu, K.-C. & Wang, Y. (2007). Experimental verification of a wireless sensing and control system for structural control using MR dampers. *Earthquake Engineering and Structural Dynamics*, Vol. 36, No. 10, (August 2007) 1303-1328, ISSN 0098-8847
- MacKay, D. J. C. (1992a). A practical Bayesian framework for backprop networks. *Neural Computation*, Vol. 4, No. 3, (May 1992) 448-472, ISSN 0899-7667
- MacKay, D. J. C. (1992b). Bayesian interpolation. *Neural Computation*, Vol. 4, No. 3, (May 1992) 415-447, ISSN 0899-7667
- Marquardt, D. W. (1963). An algorithm for least-squares estimation of nonlinear parameters. *Journal of the Society for Industrial and Applied Mathematics*, Vol. 11, No. 2, (June 1993) 431-441, ISSN 0368-4245
- Ni, Y. Q.; Chen, Y.; Ko, J.M. & Cao, D.Q. (2002). Neuro-control of cable vibration using semi-active magneto-rheological dampers. *Engineering Structures*, Vol. 24, No. 3, (March 2002) 295-307, ISSN 0141-0296
- Or, S. W.; Duan, Y. F.; Ni, Y. Q.; Chen, Z. H. & Lam, K. H. (2008). Development of magnetorheological dampers with embedded piezoelectric sensors for structural vibration control. *Journal of Intelligent Material Systems and Structures*, Vol. 19, No. 11, (November 2008) 1327-1338, ISSN 1045-389X
- Schurter, K. C. & Roschke, P. N. (2000). Fuzzy modeling of a magnetorheological damper using ANFIS. *Proceedings of the Ninth IEEE International Conference on Fuzzy Systems*, Vol. 1, pp. 122-127, ISBN 0-7803-5877-5, San Antonio, TX, May 2000, IEEE, Piscataway
- Schurter, K. C. & Roschke, P. N. (2001). Neuro-fuzzy control of structures using acceleration feedback. *Smart Materials and Structures*, Vol. 10, No. 4, (August 2001) 770-779, ISSN 0964-1726
- Song, X.; Ahmadian, M.; Southward, S. & Miller, L. R. (2005). An adaptive semiactive control algorithm for magnetorheological suspension systems. *Journal of Vibration and Acoustics*, Vol. 127, No. 5, (October 2005) 493-502, ISSN 1048-9002
- Spencer, B. F. Jr.; Dyke, S. J.; Sain, M. K. & Carlson, J. D. (1997). Phenomenological model for magnetorheological dampers. *Journal of Engineering Mechanics*, Vol. 123, No. 3, (March 1997) 230-238, ISSN 0733-9399
- Suykens, J. A. K., Vandewalle, J. P. L. & De Moor, B. L. R. (1996). *Artificial Neural Networks for Modeling and Control of Non-linear Systems*, Kluwer Academic, ISBN 0-7923-9678-2, Boston
- Tsang, H. H.; Su, R. K. L. & Chandler, A. M. (2006). Simplified inverse dynamics models for MR fluid dampers. *Engineering Structures*, Vol. 28, No. 3, (February 2006) 327-341, ISSN 0141-0296
- Wang, D.-H. & Liao, W.-H. (2001). Neural network modeling and controllers for magnetorheological fluid dampers, *Proceedings of the 10th IEEE International Conference on Fuzzy Systems*, pp. 1323-1326, ISBN 0-7803-7293-X, Melbourne, Australia, December 2001, IEEE, Piscataway.

- Weber, F.; Distl, H.; Feltrin, G. & Motavalli, M. (2005a). Evaluation procedure of decay measurements of a cable with passive-on operating MR damper, *Proceedings of the Sixth International Symposium on Cable Dynamics*, pp. 143-150, Charleston, USA, September 2005, AIM, Liège
- Weber, F.; Distl, H.; Feltrin, G. & Motavalli, M. (2005b). Simplified approach of velocity feedback for MR dampers on real cable-stayed bridges, *Proceedings of the Sixth International Symposium on Cable Dynamics*, pp. 107-114, Charleston, USA, September 2005, AIM, Liège
- Wereley, N. M.; Pang, L. & Kamath G. M. (1998). Idealized hysteresis modeling of electrorheological and magnetorheological dampers. *Journal of Intelligent Material Systems and Structures*, Vol. 9, No. 8, (August 1998) 642-649, ISSN 1045-389X
- Xia, P.-Q. (2003). An inverse model of MR damper using optimal neural network and system identification. *Journal of Sound and Vibration*, Vol. 266, No. 5, (October 2003) 1009-1023, ISSN 0022-460X
- Zhou, L.; Chang, C.-C. & Wang, L.-X. (2003). Adaptive fuzzy control for nonlinear building-magnetorheological damper system. *Journal of Structural Engineering*, Vol. 129, No. 7, (July 2003) 905-913, ISSN 0970-0137



## **Vibration Control**

Edited by Mickaël Lallart

ISBN 978-953-307-117-6

Hard cover, 380 pages

**Publisher** Sciyo

**Published online** 18, August, 2010

**Published in print edition** August, 2010

Vibrations are a part of our environment and daily life. Many of them are useful and are needed for many purposes, one of the best example being the hearing system. Nevertheless, vibrations are often undesirable and have to be suppressed or reduced, as they may be harmful to structures by generating damages or compromise the comfort of users through noise generation of mechanical wave transmission to the body. the purpose of this book is to present basic and advanced methods for efficiently controlling the vibrations and limiting their effects. Open-access publishing is an extraordinary opportunity for a wide dissemination of high quality research. This book is not an exception to this, and I am proud to introduce the works performed by experts from all over the world.

### **How to reference**

In order to correctly reference this scholarly work, feel free to copy and paste the following:

Y.Q. Ni and Z.H. Chen (2010). A Magnetorheological Damper with Embedded Piezoelectric Force Sensor: Experiment and Modeling, *Vibration Control*, Mickaël Lallart (Ed.), ISBN: 978-953-307-117-6, InTech, Available from: <http://www.intechopen.com/books/vibration-control/a-magnetorheological-damper-with-embedded-piezoelectric-force-sensor-experiment-and-modeling>

**INTECH**  
open science | open minds

### **InTech Europe**

University Campus STeP Ri  
Slavka Krautzeka 83/A  
51000 Rijeka, Croatia  
Phone: +385 (51) 770 447  
Fax: +385 (51) 686 166  
[www.intechopen.com](http://www.intechopen.com)

### **InTech China**

Unit 405, Office Block, Hotel Equatorial Shanghai  
No.65, Yan An Road (West), Shanghai, 200040, China  
中国上海市延安西路65号上海国际贵都大饭店办公楼405单元  
Phone: +86-21-62489820  
Fax: +86-21-62489821

© 2010 The Author(s). Licensee IntechOpen. This chapter is distributed under the terms of the [Creative Commons Attribution-NonCommercial-ShareAlike-3.0 License](#), which permits use, distribution and reproduction for non-commercial purposes, provided the original is properly cited and derivative works building on this content are distributed under the same license.